JACS
JOURNAL OF THE AMERICAN CHEMICAL SOCIETY

ARTICLE

pubs.acs.org/JACS

Two-Dimensional Packing of Short DNA with Nonpairing Overhangs in Cationic Liposome−DNA Complexes: From Onsager Nematics to Columnar Nematics with Finite-Length Columns

Nathan F. Bouxsein,[†,‡,§,⊥] Cecília Leal,[†,‡,§,⊥] Christopher S. McAllister,[§,⊥,#] Kai K. Ewert,[†,‡,§,⊥] Youli Li,[∥] Charles E. Samuel,[§,⊥] and Cyrus R. Safinya*[,†,‡,§,⊥]

[†]Materials Department, [‡]Physics Department, [§]Molecular, Cellular, and Developmental Biology Department, [⊥]Biomolecular Science and Engineering Program, and [∥]Materials Research Laboratory, University of California, Santa Barbara, California 93106, United States

Supporting Information

ABSTRACT: We report the formation of liquid crystalline (LC) phases of short double-stranded DNA with nonpairing (nonsticky) overhangs, confined between two-dimensional (2D) lipid bilayers of cationic liposome−DNA complexes. In a landmark study (*Science* **2007**, *318*, 1276), Nakata et al. reported on the discovery of strong end-to-end stacking interactions between short DNAs (sDNAs) with blunt ends, leading to the formation of 3D nematic (N) and columnar LC phases. Employing synchrotron small-angle X-ray scattering, we have studied the interplay between shape anisotropy-induced and DNA end-to-end interaction-induced N ordering for 11, 24, and 48 bp sDNA rods with single-stranded oligo-thymine (T) overhangs modulating the end-to-end interactions. For suppressed stacking interactions with 10-T overhangs, the volume fraction of sDNA at which the 2D isotropic (I)-to-N transition occurs for 24 and 48 bp sDNA rods depended on their length-to-width (L/D) shape anisotropy, qualitatively consistent with Onsager's theory for the entropic alignment of rigid rods. As the overhang length is reduced from 10 to 5 and 2 T for 24 and 48 bp sDNA, the N-to-I transition occurs at lower volume fractions, indicating the onset of some degree of end-to-end stacking interactions. The 11 bp sDNA rods with 5- and 10-T overhangs remain in the I phase, consistent with their small shape anisotropy ($L/D \approx 1.9$) below the limit for Onsager LC ordering. Unexpectedly, in contrast to the behavior of 24 and 48 bp sDNA, the end-to-end interactions between 11 bp sDNA rods with 2-T overhangs set in dramatically, and a novel 2D columnar N phase (N_C) with finite-length columns formed. The building blocks of this phase are comprised of 1D stacks of (on average) four 11 bp DNA-2T rods with an effective $L_{stacked}/D \approx 8.2$. Our findings have implications for the DNA-directed assembly of nanoparticles on 2D platforms via end-to-end interactions and in designing optimally packed LC phases of short anisotropic biomolecules (such as peptides and short-interfering RNAs) on nanoparticle membranes, which are used in gene silencing and chemical delivery.

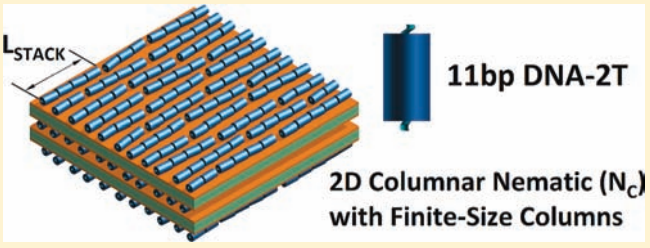

INTRODUCTION

The design of optimally packed liquid crystalline (LC) phases of anisotropic rods (including short RNA or peptides) in complexes based on cationic liposomes (CLs, closed spherical membranes) is of special interest because CLs have broad applications as carriers of therapeutic macromolecules. The experimental studies described in this paper were designed to explore and discover the conditions required for short double-stranded DNA (sDNA) to spontaneously assemble into LC phases when confined in two dimensions. While a large variety of LC phases and their phase transitions have been studied in bulk and in three-dimensional (3D) systems over the past few decades, far fewer experiments have addressed LC phase formation in well-defined 2D systems.[1,2] In our studies confinement was induced through the self-assembly of nucleic acids with CLs.[3,4] Short nucleic acid (double-stranded DNA or RNA) rods electrostatically adsorbed to oppositely charged cationic membranes[3] are ideal macromolecules for such studies because of the ability to readily tune their shape anisotropy (typically measured by their aspect ratio, the ratio of length to width (L/D)) by varying the number of base-pairs. Previous synchrotron small-angle X-ray scattering (SAXS) studies have shown that a multilamellar phase forms when CLs comprised of lamellar phase-forming cationic and neutral lipids are mixed with long DNA chains (λ-DNA with ∼48 000 bp or plasmid DNA with ∼5000 bp). In this multilamellar phase (termed L_α^C), DNA chains are intercalated between cationic lipid bilayers.[5,6] Quantitative line shape analysis of the DNA−DNA correlation peak has shown that the DNA chains form a finite-size 2D smectic phase.[7,8] In these systems, the interhelical distance between DNA chains (and thus the effective DNA volume fraction confined between membranes) may be readily tuned by simply varying the membrane charge density.[4,5,7−10]

Onsager was the first to describe the type of phases expected to form with increasing volume fraction (packing density) of

Received: March 7, 2011
Published: April 26, 2011

dx.doi.org/10.1021/ja202082c | *J. Am. Chem. Soc.* 2011, 133, 7585–7595

anisotropic macromolecules. In a landmark paper on LC phase formation,[11] Onsager showed that anisotropic, hard-core repulsive molecules with length L and diameter D dispersed in solvent will undergo an entropy-driven phase transition from the isotropic (I) phase, where the long axes of the molecules are randomly oriented (Figure 1A), to a nematic (N) phase,[1,2] where the long axes of the molecules are preferentially oriented along a common direction (Figure 1B), if $\Phi_V^{rod} \geq \Phi^* = 4D/L$. Here, Φ_V^{rod} is the volume fraction of rods, which implies that N phase formation requires $L/D \geq 4$ since volume fractions cannot be larger than 1. Although the N phase has long-range orientational order, it only exhibits short-range positional order.[1,2] The N phase forms because the gain in translational entropy is larger than the loss of orientational entropy of the rods, resulting in a net gain in entropy of the N phase compared to the I phase for $\Phi_V^{rod} \geq \Phi^*$ (i.e., at concentrations above Φ^*, rods can translate past each other in the N phase but not in the I phase). If the rods are monodisperse, one may expect a further transition at even higher packing densities to the smectic-A phase, with rods segregated into layers with quasi-long-range positional order.[1,2] Although Onsager's original paper[11] examined anisotropic objects in the limit where L was much larger than D, recent computer simulations of anisotropic objects are in qualitative agreement with the Onsager condition for LC ordering, even in the limit where L/D is of order 4. In computer simulation studies of a 3D system of cylinders with spherical caps, the nematic phase formed for $L/D > 4.7$.[12] Monte Carlo simulations of 2D hard ellipses show the I, N, and smectic-A phases for shape aspect ratios a/b of 4 and 6, but only the isotropic phase for $a/b = 2$, where a and b are the major and minor axes of the ellipse, respectively.[13,14] In these latter simulations, the I-to-N phase transition appears to be continuous for $a/b = 6$ and first-order for $a/b = 4$.

In an unexpected finding related to Onsager's theory, recent pioneering work on concentrated solutions of very short DNA revealed deviating LC phase behavior.[15,16] DNA as short as 6 bp with $L/D \approx 1$ (hydrated B-DNA has a length of 3.4 Å per base pair and a diameter of 20 Å) spontaneously organized into 3D nematic and columnar phases, thus contradicting the Onsager criterion for LC formation. These phases of short DNA[15] were similar to those found for long DNA in solution.[17,18] This provided strong experimental evidence that the short, blunt-ended DNA double-strands were spontaneously stacking end-to-end to minimize exposure of the internal hydrophobic core to the aqueous environment.[15,16] The effective length (L_{eff}) of the stacked duplexes (proportional to the number of duplexes in a stack) resulted in L_{eff}/D much larger than 4, and at sufficient concentrations even very short DNA duplexes then satisfied the Onsager criterion for nematic ordering.[11]

We studied sDNA molecules containing nonpairing (nonsticky) overhangs at the ends of the duplexes to explore their 2D LC phase behavior. The nonsticky overhangs of varied length modulated the DNA end-to-end stacking interactions discovered by Nakata et al.[15] The sDNA rods were confined between bilayer membranes in the lamellar phase of CL−sDNA complexes (Figure 1), and their volume fraction was varied by changing the charge density of the membranes. The structure and phase behavior of the CL−sDNA complexes was determined using synchrotron SAXS. We chose three different lengths for the duplex section of sDNA molecules (11, 24, and 48 bp), corresponding to L/D ratios (1.87, 4.08, and 8.16) below, at, and above the required Onsager criterion for nematic phase formation (see Table 1). The nonsticky ends consisted of 2, 5, or 10

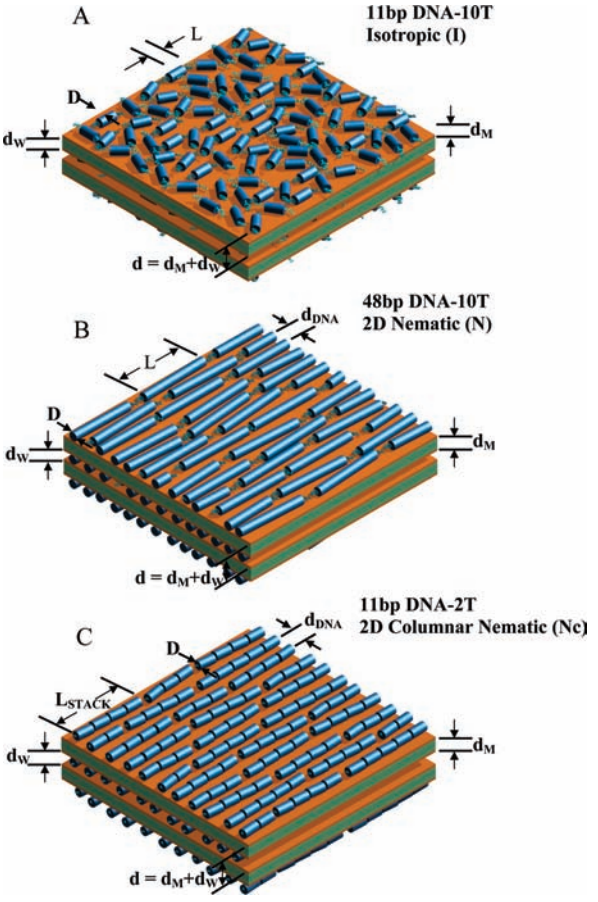

Figure 1. Schematic drawings of the distinct packing phases of sDNA rods (all of which contain nonsticky overhangs) in cationic liposome−short DNA (CL−sDNA) complexes. The complexes are multilamellar assemblies of alternating cationic lipid bilayers of thickness d_M and water layers of thickness d_W. The water layer contains a monolayer of sDNA molecules. The multilamellar unit cell dimension is $d = d_W + d_M$. (A) Isotropic phase with short-range positional and orientational order, as observed for 11 bp DNA-10T (11 bp DNA core with a 10-T nonsticky overhang at each end), with small shape anisotropy (length/width = $L/D \approx 1.9$). (B) Nematic LC phase, as observed for 48 bp DNA rods with nonsticky ends ($L/D \approx 8.16$). Formation of this phase by sDNA rods with sufficiently anisotropic shape is consistent with Onsager's model of LC ordering of anisotropic rods. For 5- and 2-T nonsticky ends, some transient dimers may form, indicating the onset of sDNA end-to-end interactions. All rods are the same length (apparently shorter rods are shown cut off at the edges). (C) New type of 2D columnar nematic phase, as observed for 11 bp DNA-2T rods. The onset of strong DNA end-to-end interactions for 11 bp DNA with very short (2 T) nonsticky overhangs leads to the formation of a distribution of 1D stacks of sDNA rods, which become the building blocks of the nematic phase. The 1D stacks have an average size of ~4 rods, corresponding to an effective length to width ratio $L/D \approx 7.3$. In parts B and C, d_{DNA} corresponds to the average interhelical spacing. The "Onsager nematic" (N) (part B) and columnar nematic (N_C) (part C) phases exhibit long-range orientational and short-range positional order. The drawings are not meant to imply that the orientation of sDNA rods is correlated between layers.

additional desoxynucleotides with the base thymine (T) at the 3′-end of each DNA strand in the sDNA duplex. The addition of 10 nonpairing nucleotides strongly suppressed DNA end-to-end interactions. In accordance with Onsager's predictions (where ordering is dependent upon the volume fraction of the confined

Table 1. Nucleic Acid Shape Anisotropy for the Base-Paired Sections of the Short DNA Molecules Studied[a]

	length (Å)	L/D
11 bp DNA	37	1.87
24 bp DNA	81.6	4.08
48 bp DNA	163.2	8.16

[a] The length-to-width ratio (L/D) is for DNA in the hydrated B-conformation with a 3.4 Å rise per base pair and a diameter of 20 Å.

sDNA molecules as well as their anisotropic shape), the 11 bp DNA-10T only exhibited the I phase, while 48 bp DNA-10T and 24 bp DNA-10T sDNA formed N phases (Figure 1B). The DNA end-to-end interactions set in gradually for 48 and 24 bp sDNAs containing 5- and 2-T nonsticky ends, which slightly shifts the phase boundaries. In contrast, the phase behavior of 11 bp sDNA varied more drastically. While 11 bp DNA rods with 10- and 5-T overhangs exhibited only the predicted I phase (Figure 1A), rods with 2-T nonsticky ends exhibited a 2D N phase with very strong short-range positional correlations. This highly correlated 2D N phase melted into the I phase at relatively small DNA volume fractions. These findings suggest that strong end-to-end interactions of 11 bp DNA-2T rods give rise to a new type of columnar N phase (labeled N_C) where the effective "building blocks" consist of 1D stacks of about four 11 bp DNA-2T duplexes with $L_{stacked}/D \approx 8.2$, well above the minimum shape anisotropy required by Onsager's theory (Figure 1C).

The discovery of 2D LC phases of anisotropic rods reported in this paper is expected to have broad implications in the design of optimally packed delivery vectors for small anisotropic molecules (such as active peptides and small proteins and short-interfering RNA (siRNA)) for applications in bionanotechnology, chemical delivery, and gene silencing.[3,19,20] In particular, for siRNA used in gene silencing,[3,20] stacking of these very short rods with $L/D \approx 2$ should yield CL−siRNA complexes where oriented stacks of siRNA optimally pack in the nematic phase, requiring less lipid. We note that siRNA is comprised of dsRNA in the A-form, i.e., a right-handed helix conformation with a diameter of 26 Å and a rise per base pair of 2.6 Å. Thus, for core sizes ranging between 19 and 23 bp with two nucleotide 3′ overhangs, $L/D \approx 2$, well below the Onsager condition for nematic formation.

In addition, our findings have important implications in the general area of DNA-based assembly in nanotechnology.[21−25] To date, all DNA-directed assembly/crystallization of colloidal particles (such as metallic or nonmetallic nanoparticles with optical and optoelectronic properties) into larger scale materials has been based on recognition through H-bonding of complementary base pairs. The described methods involve joining building blocks together through complementary (sticky) ends tethered to opposing surfaces, or via noncomplementary projecting domains bridged by an intermediate oligonucleotide with sticky ends. In contrast, the results presented in this paper offer a new direction in DNA-based directed assembly on a 2D substrate platform, where tunable end-to-end stacking interactions (i.e., with either moderate stacking interactions for 24 and 48 bp sDNA with 5- and 2-T overhangs or significantly larger stacking interactions for 11 bp DNA-2T) would join building blocks containing short base pairs tethered to their surfaces.

MATERIALS AND METHODS

DNA Constructs. All DNA constructs were purchased as single strands from Sigma-Genosys (Sigma-Aldrich) and delivered as a lyophilized film. These oligos where fully deprotected, leaving hydroxy ends, and desalted. HPLC was used to purify oligos >30 nucleotides (nts). The films were centrifuged to collect all dried components and then resuspended in 10 mM HEPES buffer (pH = 7.0) to ∼10 mg/mL. Concentrations were determined by UV absorption using a ND-1000 UV−vis spectrophotometer from NanoDrop Technologies (Thermo Fisher Scientific). Equimolar amounts of complementary single strands were mixed and diluted to a final concentration of 10 mg/mL. Mixed single strands were heated in a water bath and held at 90 °C for 15 min. The nucleic acids were then slowly cooled to room temperature to facilitate complete hybridization. Duplexes were run on a 12% polyacrylamide gel to check for single-stranded DNA contaminants. DNA sequences are listed in Table S1 in the Supporting Information. The chosen sequences correspond to the siRNA sequence described previously[3] and flank the targeted mRNA sequence from the firefly genome commonly used as a reporter in gene silencing experiments.[26]

Liposome Preparation. The lipids 2,3-dioleyloxypropyltrimethylammonium chloride (DOTAP, "1,2-dioleoyl-3-trimethylammonium-propane") and 1,2-dioleoyl-*sn*-glycero-3-phosphatidylcholine (DOPC) were purchased from Avanti Polar Lipids as lyophilized powders and dissolved in chloroform at 30 mM. These stock solutions were mixed at molar ratios (DOTAP:DOPC) of 100:00, 90:10, 80:20, 70:30, 60:40, 50:50, 40:60, 30:70, and 20:80 in glass vials (to yield Φ_{NL} = 0.0, 0.1, 0.2, 0.3, 0.4, 0.5, 0.6, 0.7, and 0.8, respectively). The chloroform was then evaporated with a stream of nitrogen to produce a lipid film inside the vial, which was further dried in a vacuum (rotary vane pump) for 24 h. Lipid films were then rehydrated with high-resistivity water (18.2 MΩ cm) to a final concentration of 30 mM total lipid at 37 °C. The resulting liposome solutions were sonicated with with a Vibra-Cell tip sonicator (Sonics & Materials) for 10 min and immediately stored at 4 °C until use.

SAXS Experiments. CL−sDNA complexes for X-ray diffraction were prepared as described previously.[3] All samples were prepared to be stoichiometrically neutral, i.e., at the isoelectric point of the CL−DNA complex with cationic to anionic charge ratio $\rho_{chg} = N+/N- = N_{CL}/N_{nt} = 1$. Here, $N+$ and $N-$ are the numbers of positive (lipid) and negative (DNA) charges, respectively, and N_{CL} and N_{nt} are the amounts (in mol) of cationic lipid (univalent DOTAP bearing one positive charge) and nucleotides (bearing one negative charge each) in the sample, respectively. A total of 50 μg of DNA per sample was added into quartz X-ray capillaries (Hilgenberg) as a solution containing 4−8 mg/mL DNA. The appropriate amount of liposome solution was added, and capillaries were centrifuged at 1500*g* for 15 min at 4 °C to pellet the resulting complex. Capillaries were sealed and stored at 4 °C until use. SAXS experiments were performed at the Stanford Synchrotron Radiation Lightsource, beamline 4-2, using a 1.5 m flight path with X-ray energy set to 9 keV. Data were collected on a MX-225 Rayonix CCD detector and radially averaged to produce 1D intensity versus wave-vector (q) plots. Structural parameters were derived from SAXS profiles by line shape fitting as described in the text. Data with error bars in the plots of the structural parameters indicate the average and standard deviation of fit results for complexes that were prepared more than once.

RESULTS AND DISCUSSION

Choice of DNA Constructs and Lipids. In order to probe the effect of rod length and end-to-end interactions on the ordering of sDNA in CL−sDNA complexes, we first chose three different lengths for the duplex section of the sDNA molecules. As shown in Table 1, these lengths (11, 24, and 48 bp) correspond to L/D

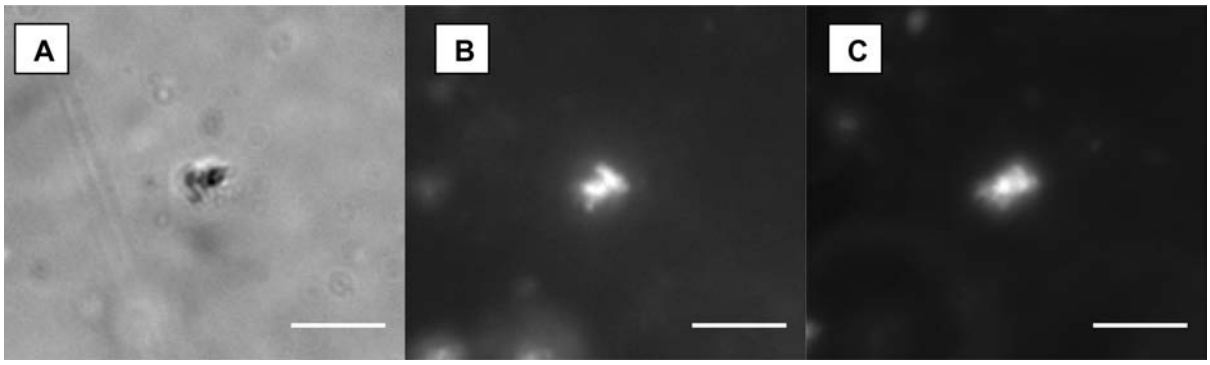

Figure 2. Optical microscopy of CL−sDNA complexes. The colocalization of lipid and DNA label demonstrates complex formation. (A) Differential interference contrast image of a CL−11 bp DNA-10T complex. (B) The same complex imaged in fluorescence mode showing the lipid label (Texas Red-DHPC). (C) The same complex imaged in fluorescence mode showing the DNA label (Cy5). Scale bars, 10 μm.

ratios (1.87, 4.08, and 8.16, respectively) below, at, and above the Onsager criterion for nematic phase formation. To modulate the end-to-end stacking interactions, each of these sDNAs was prepared with nonsticky ends of 2, 5, or 10 desoxynucleotides with the base thymine (T) at the 3′-end of each DNA strand in the sDNA duplex (see Table S1 in the Supporting Information for the sDNA sequences). As lipids, we chose the well-studied DOTAP/DOPC system,[4−9] which allows tuning of the membrane charge density and thus the sDNA volume fraction.

Figure 2 shows optical micrographs of a CL−11 bp DNA-10T complex. Complexes are clearly visible in the differential interference contrast mode as micrometer-size particles, and colocalization of fluorescent lipid and DNA labels unambiguously demonstrates complex formation. We used synchrotron SAXS to study the phase behavior of the sDNAs confined in these complexes.

Shape Anisotropy-Induced 2D Onsager Nematic Phases of Short DNA Duplexes. *SAXS Studies of CL Complexes of sDNAs with 10-T Overhangs.* Short DNA molecules consisting of a core duplex of 11, 24, or 48 bp with 10-T single-strand overhangs at each end (11 bp DNA-10T, 24 bp DNA-10T, and 48 bp DNA-10T, respectively) were complexed with cationic DOTAP/DOPC liposomes at $\rho_{chg} = 1$. SAXS profiles of these complexes at a variety of Φ_{NL} (mole fraction of neutral lipid DOPC) are shown in Figure 3. The sharp Bragg peaks arise from the (00L) reflections of the multilamellar structure of the CL−sDNA complexes (Figure 1), as observed in complexes incorporating long λ-DNA.[5,7−9] The CL−sDNA complexes exhibit a single-phase multilamellar structure for Φ_{NL} from 0 up to 0.7, beyond which the lipid mixture phase-separates. In the displayed q-range the (001) and (002) reflections are visible in all SAXS profiles. In some cases, peaks up to the (004) reflection are detected, e.g., in the top profile in Figure 3B. The (003) reflection is close to a minimum of the X-ray form factor and therefore weak.

At $\Phi_{NL} = 0$ for 24 bp DNA-10T and 48 bp DNA-10T (bottom SAXS profiles, Figure 3B,C), the two sharp peaks at $q_{001} = 0.11$ Å^{-1} and $q_{002} = 0.22$ Å^{-1} yield an interlayer spacing $d = d_M + d_W = L(2\pi/q_{00L}) = 57$ Å. Here, d_M is the membrane thickness and d_W is thickness of the water layer, which contains the sDNA rods, as shown schematically in Figure 1. For 11 bp DNA-10T, the interlayer spacing $d = 2\pi/q_{001} \approx 55.4$ Å at $\Phi_{NL} = 0$ is nearly the same. The thickness of a DOTAP bilayer d_M is ∼33 Å,[5,9] which leaves a thickness of $d_W = d - d_M \approx 24$ Å for complexes containing 24 and 48 bp DNA-10T and $d_W \approx 22.6$ Å for complexes containing 11 bp DNA-10T. This is sufficient to accommodate a monolayer of hydrated DNA in the B-conformation: without the hydration layer, B-DNA has a diameter of ∼20 Å.

A number of SAXS profiles (at $\Phi_{NL} = 0$ for all samples shown in Figure 3, and, in particular for 24 bp DNA-10T and 48 bp DNA-10T, over some range of Φ_{NL}) also show a broad peak resulting from short-range sDNA−sDNA correlations. The corresponding average spacing between sDNA molecules is $d_{DNA} = 2\pi/q_{sDNA}$ (lines and arrows point to the broad peaks in Figure 3). Previous line shape analysis of the DNA−DNA correlation peak in CL−DNA complexes incorporating long λ-DNA has shown that these DNA chains form a finite-size 2D smectic phase (i.e., with parallel chains spaced at d_{DNA}).[7,8] In contrast, a simple line shape analysis (described below) shows that the sDNA duplexes form a 2D nematic phase with long-range orientational order and short-range liquid-like positional order or a 2D isotropic phase with short-range orientational and positional order, depending on their length and the length of the nonsticky overhangs.[1,2]

In order to further clarify the nature of the broad sDNA−sDNA correlation peaks near the sharp (002) reflection, we performed a nonlinear least-squares fit of the data with a sum of two Lorentzians, one to fit the (002) reflection, and the other to fit the sDNA−sDNA correlation peak. The broad sDNA peak is typical of short-range positional correlations (i.e., with the real-space density pair-correlation function falling off exponentially), and we thus expected the structure factor (proportional to the Fourier transform of the density−density correlation function) to be adequately described by a Lorentzian function.[2] The X-ray structure factor describing the (00L) peaks exhibits power-law singularities because the layer−layer correlation function of the multilamellar phase exhibits only quasi-long-range positional order[27−29] due to the well-established Landau−Peierls effect,[30,31] rather than δ-function Bragg diffraction peaks characteristic of long-range order. However, for the purposes of obtaining the interlayer spacing from the peak position of any of the (00L) peaks as $d = L(2\pi/q_{00L})$, we found that a Lorentzian function was adequate.

For each peak the Lorentzian function was written as $S(q) = A/[(q - q_o)^2 + \kappa^2]$, with the fitting parameters q_o, κ, and A. Here q_o is the peak position (in Å^{-1}), κ is the half-width at half-maximum (hwhm, in Å^{-1}), and A/κ^2 is the peak intensity. For the sDNA SAXS peak, the correlation length $L_C = 1/\kappa$ is the

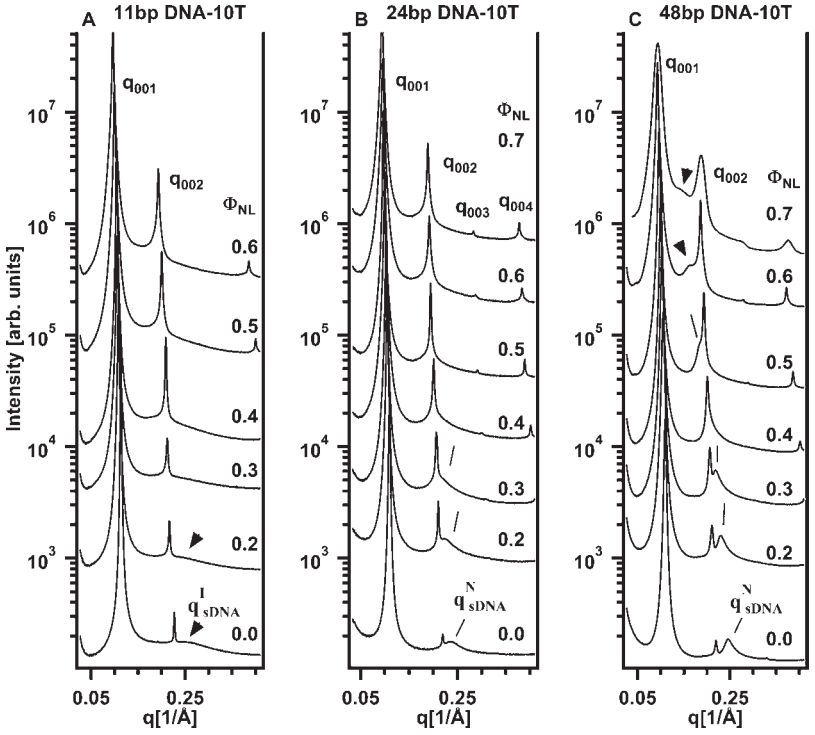

Figure 3. Synchrotron small-angle X-ray scattering (SAXS) profiles of CL−sDNA complexes as a function of neutral lipid mole fraction (Φ_{NL}) for 11, 24, and 48 bp sDNA with 10-T (thymine) nonsticky overhangs. The (00*L*) diffraction peaks result from the multilamellar structure of the complexes as described in the text. (A) For 11 bp DNA-10T (with length/width = $L/D \approx 1.9$), very broad sDNA−sDNA correlation peaks are visible for $\Phi_{NL} = 0$ and 0.2 (indicated by arrows, labeled q^{I}_{sDNA}), consistent with the 2D isotropic phase of rods (see Figure 1A) with very weak positional correlations. (B) For 24 bp DNA-10T ($L/D \approx 4.08$), the sDNA−sDNA correlation peaks (indicated by lines, labeled q^{N}_{sDNA}) are stronger (compared to the data in part A) for $\Phi_{NL} = 0$ and 0.2 (with the sDNA peak somewhat buried under the (002) reflection for $\Phi_{NL} = 0.3$). (C) For 48 bp DNA-10T ($L/D \approx 8.16$), the sDNA−sDNA correlation peaks (indicated by lines) are further enhanced (compared to the data in parts A and B). In (B) and (C) the q^{N}_{sDNA} peaks result from "Onsager nematic" phases (see Figure 1B) as described in the text.

length scale over which sDNA molecules have short-range positional correlations (i.e., the distance over which the molecules "know" of each other's presence).[32−34] A representative example of the line shape analysis of the (002) and q_{sDNA} peaks is shown in Figure 4 for CL−sDNA complexes containing 48 bp DNA-10T at $\Phi_{NL} = 0.2$. Figure 4A shows the SAXS profile and the background scattering (dashed lines), which was approximated by an exponential decay fit to the X-ray intensity far from the peaks. The high quality of the fit of the background-subtracted SAXS intensity (open circles) to the double Lorentzian model (solid line) is apparent in Figure 4B.

Figure 5 summarizes the results of the fits to the SAXS profiles of Figure 3 for 11 bp DNA-10T, 24 bp DNA-10T, and 48 bp DNA-10T. The interlayer spacing $d = d_M + d_W$ increases with increasing Φ_{NL} (Figure 5A). This behavior is due to increases in both the membrane bilayer thickness d_M (each DOPC molecule is about 4−6 Å longer than a DOTAP molecule) and the water layer (because DOPC has a larger hydration shell compared to DOTAP) as Φ_{NL} increases.[5] Figure 5B shows that the average spacing between sDNA molecules increases with Φ_{NL} (i.e., the sDNA SAXS peaks (lines and arrows in Figure 3) move to lower q with increasing Φ_{NL}). In other words, d_{DNA} grows with decreasing membrane charge density (as Φ_{NL} increases from 0 to 0.7). This trend is also observed for CL−DNA complexes containing long DNA.[5] It reflects the fact that the average cationic (membrane) charge density within the CL−sDNA complex has to match the average anionic charge density due to the sDNA to maintain local charge neutrality (assuming all counterions have been released from the complex into the surrounding solution).[5,7−9]

Calculation of the Membrane Charge Density (σ_M) and DNA−DNA Distance (d_{DNA}). The equating of cationic and anionic charge densities leads to the simple equation $\sigma_M = e/[(d_{DNA})(3.4\ \text{Å})]$, where σ_M is the cationic membrane charge density, e is the elementary charge, and 3.4 Å is the distance between two charges along the sDNA duplex.[5,9,10] The membrane charge density (total charge/total lipid area) may be written as $\sigma_M = N_{CL}eZ_{CL}/(N_{NL}a_{NL} + N_{CL}a_{CL}) = [N_{CL}/(N_{CL} + rN_{NL})]\sigma_{CL}$. Here, Z_{CL} (=1 for DOTAP) is the valence of the cationic lipid; N_{CL} and N_{NL} are the number of cationic and neutral lipids, respectively; a_{CL} and a_{NL} are the headgroup area of the cationic and neutral lipid, respectively; $r = a_{NL}/a_{CL}$; and $\sigma_{CL} = Z_{CL}e/a_{CL}$ is the charge density for the cationic lipid. For $a_{CL} = a_{NL}$ ($r = 1$), this simplifies to $\sigma_M = \Phi_{CL}\sigma_{CL} = (1 - \Phi_{NL})\sigma_{CL}$, where $\Phi_{CL} = 1 - \Phi_{NL}$ is the mole fraction of cationic lipid. Thus, $(1 - \Phi_{NL})\sigma_{CL} = e/[(d_{DNA})(3.4\ \text{Å})]$, which means that the average spacing between sDNA molecules is given by $d_{DNA} = a_{CL}/[3.4\ \text{Å}(1 - \Phi_{NL})]$. If the lipid headgroup areas are comparable but not equal, one can write $r = 1 + \varepsilon$ (with $|\varepsilon| \ll 1$), which leads to $d_{DNA} \approx a_{CL}/[3.4\ \text{Å}Z_{CL}(1 - \Phi_{NL})(1 - \varepsilon\Phi_{NL})]$ as derived in the Supporting Information (Eq. S2). For our system, taking $a_{CL} \approx 70\ \text{Å}^2$ (a standard value for singly charged amphiphiles) and $a_{NL} \approx 72\ \text{Å}^2$ (from Ahmad et al.[35]) gives $d_{DNA} \approx 34.7$, 41.8, and 52.4 Å at $\Phi_{NL} = 0.4$, 0.5, and 0.6, respectively,

dx.doi.org/10.1021/ja202082c |*J. Am. Chem. Soc.* 2011, 133, 7585–7595

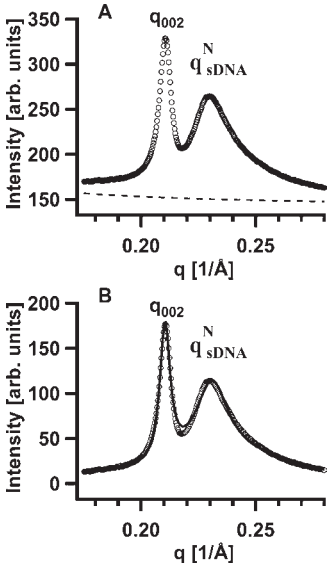

Figure 4. (A) Part of the SAXS profile for CL−sDNA complexes incorporating 48 bp DNA-10T at Φ_{NL} (neutral lipid mole fraction) = 0.2 (cf. Figure 3C). The dashed line shows the background scattering, which was approximated as an exponential decay fit through the X-ray intensity far from the diffraction peaks. (B) A nonlinear least-squares fit of the background-subtracted SAXS profile from part A (open circles) with the sum of two Lorentzians (solid line). Each Lorentzian function was written as $S(q) = A/[(q - q_o)^2 + \kappa^2]$, where q_o and κ correspond to the peak position and the hwhm, respectively. For the (002) SAXS peak, $A_{002} = 4.38 \times 10^{-3}$, $q_{002} = 0.2105$ Å^{-1}, and $\kappa_{002} = 2.69 \times 10^{-3}$ Å^{-1}, and for the q^{N}_{sDNA} SAXS peak (due to sDNA−sDNA correlations), $A_{sDNA} = 3.16 \times 10^{-2}$, $q_{sDNA} = 0.2310$ Å^{-1}, and $\kappa_{sDNA} = 9.74 \times 10^{-3}$ Å^{-1}.

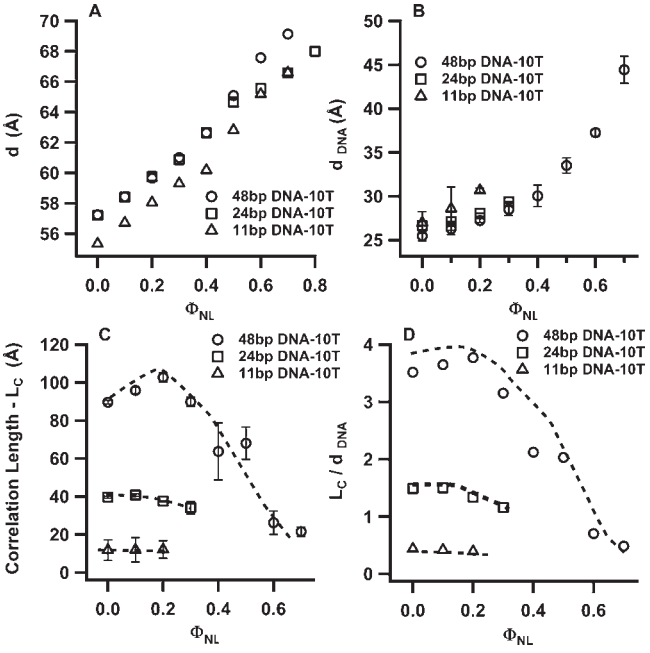

Figure 5. Plots of structural parameters for sDNAs with 10-T nonsticky ends as a function of mole fraction of neutral lipid (Φ_{NL}). The parameters were obtained from the line shape fitting of a double Lorentzian to the q_{002} and q_{sDNA} peaks in the SAXS profiles shown in Figure 3. Open triangles, squares, and circles correspond to CL−sDNA complexes incorporating 11 bp DNA-10T, 24 bp DNA-10T, and 48 bp DNA-10T, respectively. (A) Plot of the interlayer spacing d (see Figure 1) of the multilamellar structure of CL−sDNA complexes. (B) Plot of the average separation between sDNA molecules (d_{DNA}) confined between lipid bilayers. (C) Plot of the correlation length (L_C, the distance over which the centers of mass of sDNA molecules are correlated). L_C was obtained as the inverse of the hwhm of the sDNA−sDNA correlation peaks. (D) Plot of the correlation length in units of the distance between sDNA molecules (L_C/d_{DNA}). While values of L_C/d_{DNA} larger than 1 are typical for the nematic phase, values of less than 1 indicate the isotropic phase with little correlations.

while the experimental data give 29, 33, and 37.5 Å. Thus, matching the anionic/cationic charge densities in the complex predicts the trend observed in Figure 5B, where d_{DNA} increases with increasing Φ_{NL}. The systematic differences between the data and model may be due to the oversimplified assumption that all counterions are released after CLs and sDNA are mixed to form the multilamellar CL−sDNA complex. Retention of a fraction of the counterions within the complex (predicted by analytical theories of CL−DNA complexes[36]) would screen the interheadgroup repulsion and decrease a_{CL}. This effect, in turn, would reduce the measured values of d_{DNA}. We note that as Φ_{NL} tends to zero (where the membrane charge density is at its maximum), the resulting most compressed spacing between DNA rods will approach the repulsive hard-core interaction between hydrated DNA rods in their B-conformation of ∼25 Å. In this regime, hydration repulsion between DNA rods (which are not taken into account in the above calculation of d_{DNA}) will compete with the electrostatic forces.

Determination of sDNA Phases Using the Correlation Length (L_C). Figure 5C shows a plot of the sDNA−sDNA correlation length L_C for 11 bp DNA-10T, 24 bp DNA-10T, and 48 bp DNA-10T as a function of Φ_{NL}. In order to express over how many neighbors the DNA rods are correlated to each other, Figure 5D shows the same data in units of the average d_{DNA} spacing. The data are quite revealing. For 11 bp DNA-10T (open triangles) $L_C/d_{DNA} < 1$, implying essentially no correlations between sDNA rods confined in the volume of water between two lipid bilayers. This is indicative of a 2D isotropic (I) phase of sDNA adsorbed between cationic membranes (Figure 1A).

In contrast, L_C/d_{DNA} extends between 2 and 3.5 neighbors for 48 bp DNA-10T (open circles) at $\Phi_{NL} < 0.5$, signifying enhanced short-range order typical of a 2D nematic (N) phase.[32−34] For this sDNA, L_C/d_{DNA} is less than 1 for $\Phi_{NL} = 0.6$ and 0.7, indicating a 2D N-to-I phase transition for $0.5 < \Phi_{NL} < 0.6$. For the 24 bp DNA-10T of intermediate length, L_C/d_{DNA} is between 1 and 2 for $\Phi_{NL} < 0.3$, consistent with a weak N phase. For $\Phi_{NL} > 0.3$, the absence of a sDNA−sDNA correlation peak indicates the presence of the 2D I phase. As we describe below, this observed phase behavior (for sDNA rods with relatively long 10-T nonsticky ends) is consistent with Onsager's predictions, which correlate the shape anisotropy of the sDNA rods with the onset of the N−I phase transition as a function of Φ_{NL}.

Calculation of the sDNA Volume Fraction as a Function of Φ_{NL}. To compare our experimental results to Onsager's theory, we need to devise an expression for the volume fraction of sDNA in terms of the mole fractions of cationic and neutral lipid. We first derive this at $\Phi_{CL} = 1$, i.e., in the absence of neutral lipid. The small thickness of the water layer (approximately equal to the diameter of a DNA rod) confines the DNA rods in two dimensions, and the rods electrostatically adhere to the top and bottom membranes. Thus, their projected areas do not interpenetrate. Accordingly, the volume fraction of sDNA rods

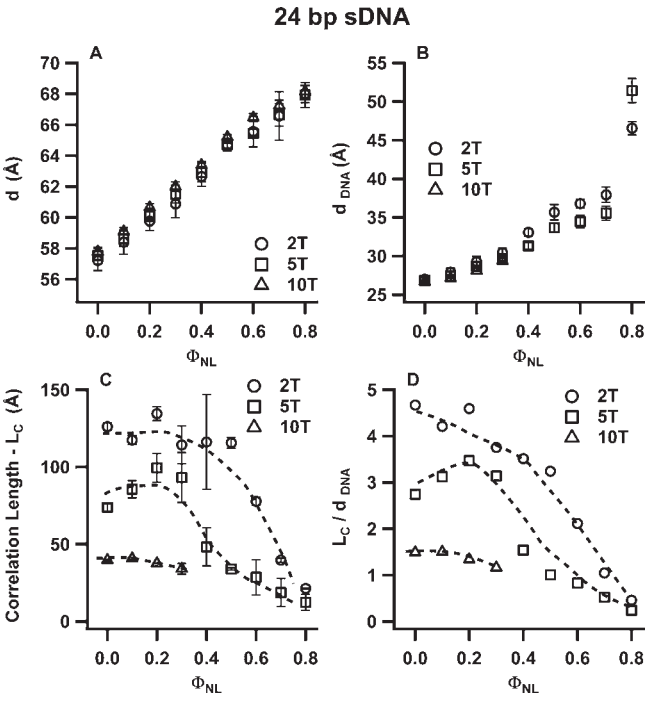

Figure 6. Structural parameters of CL−sDNA complexes incorporating 24 bp DNA-2T (open circles), 24 bp DNA-5T (open squares), and, for comparison, 24 bp DNA-10T (open triangles) from Figure 5 as a function of Φ_{NL}. The parameters result from line shape fits of the q_{002} and q_{sDNA} peaks in the SAXS profiles of the corresponding complexes (incorporating 24 bp DNA-2T and 24 bp DNA-5T) with a double Lorentzian, as illustrated in Figure 4. The plots show the interlayer spacing d (A), the average spacing (d_{DNA}) between sDNA molecules (B), the correlation length L_C (C), and L_C in units of d_{DNA} (D). The data show that the correlation length increases as the length of the nonsticky ends on the 24 bp core duplex decreases from 10 to 5 and 2 T. The range of Φ_{NL} values for which $L_C/d_{DNA} > 1$ (the nematic phase regime) also increases systematically going from 5- to 2-T overhangs. This behavior indicates the onset of a moderate amount of sDNA end-to-end interactions.

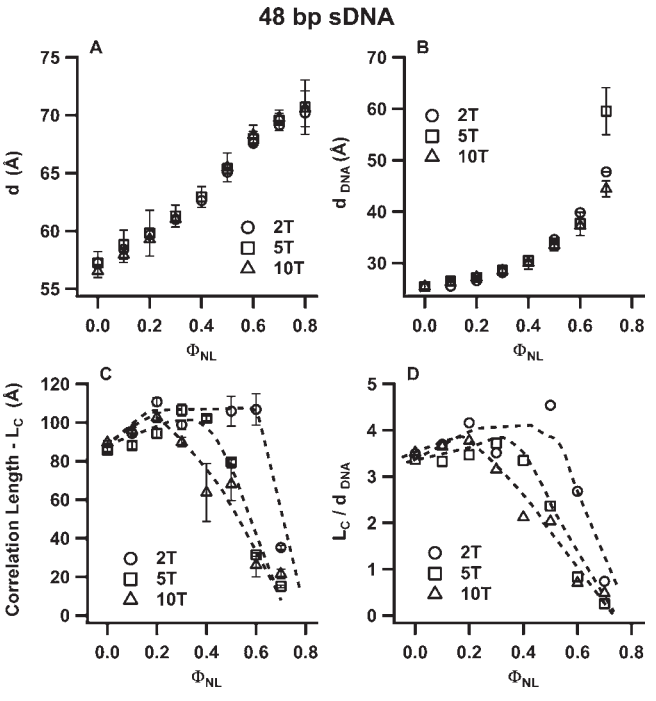

Figure 7. Structural parameters of CL−sDNA complexes incorporating 48 bp DNA-2T (open circles), 48 bp DNA-5T (open squares), and, for comparison, 48 bp DNA-10T (open triangles) from Figure 5 as a function of Φ_{NL}. The parameters result from line shape fits of the q_{002} and q_{sDNA} peaks in the SAXS profiles of the corresponding complexes (incorporating 48 bp DNA-2T and 48 bp DNA-5T) with a double Lorentzian. The plots show the interlayer spacing d (A), the average spacing (d_{DNA}) between sDNA molecules (B), the correlation length L_C (C), and L_C in units of d_{DNA} (D). Similar to the data shown in Figure 6 (for 24 bp DNA with 5- and 2-T overhangs), both the correlation length and the range of Φ_{NL} values for which $L_C/d_{DNA} > 1$ (indicative of the nematic phase) increase as the length of the nonsticky overhangs for 48 bp DNA is reduced from 10 to 5 and 2 T. This behavior results from the onset of sDNA end-to-end interactions.

within the water layer between the lipid membranes is given by ${\Phi_V}^{sDNA}(\Phi_{CL} = 1)$ = (volume of sDNA in water layer)/(volume of water layer bound by membrane), where the volume of sDNA is the effective excluded volume, consisting of the projected area of the sDNA onto the membrane surface times the water layer thickness d_W. We can then write ${\Phi_V}^{sDNA}(\Phi_{CL} = 1) = A_{sDNA}d_W/0.5A_{CL}d_W = A_{sDNA}/0.5A_{CL} = 2(N_{sDNA}/N_{CL})(a_{sDNA}/a_{CL})$. Here, $A_{sDNA} = N_{sDNA}a_{sDNA}$ is the total area of sDNA molecules projected onto the lipid membrane; N_{sDNA} is the number of sDNA molecules; a_{sDNA} is the area of one sDNA molecule projected onto lipid membrane; and A_{CL} is the total area of the membrane. The factor of 0.5 arises because of the geometry of the lamellar phase, where the water layer is bound by two membrane layers, one above it and one below it. Expressing ${\Phi_V}^{sDNA}$ in terms of the cationic/anionic charge ratio $\rho_{chg} = N_{CL}/N_{nt} = (N_{CL}Z_{CL})/(N_{sDNA}Z_{sDNA})$, where Z_{sDNA} is the valence (number of nucleotides) of the sDNA, we obtain ${\Phi_V}^{sDNA}(\Phi_{CL} = 1) = (2/\rho_{chg})(a_{sDNA}/Z_{sDNA})(Z_{CL}/a_{CL})$. If we approximate the combined projected area of the two nonsticky overhangs with the area they would occupy if they were paired with each other, we get $a_{sDNA}/Z_{sDNA} \approx N_{bp}a_{bp}/2N_{bp} = a_{bp}/2$, where N_{bp} is the number of base pairs in the sDNA (including the only hypothetically paired overhangs) and a_{bp} is the area of base pair projected onto the lipid membrane. The expression for the volume fraction then simplifies to

$$ {\Phi_V}^{sDNA}(\Phi_{CL} = 1) = (Z_{CL}/\rho_{chg})(a_{bp}/a_{CL}) \qquad (1) $$

For $\Phi_{NL} \neq 0$, the addition of neutral lipid expands the total lipid area from $N_{CL}a_{CL}$ to $N_{CL}a_{CL} + N_{NL}a_{NL}$ and therefore decreases the sDNA volume fraction by a corresponding factor of $(N_{CL}a_{CL})/(N_{CL}a_{CL} + N_{NL}a_{NL}) = N_{CL}/(N_{CL} + rN_{NL})$, with $r = a_{NL}/a_{CL}$ as defined previously. For $r = 1 + \varepsilon$ (with $|\varepsilon| \ll 1$), this factor may be written as $N_{CL}/(N_{CL} + rN_{NL}) \approx \Phi_{CL}(1 - \varepsilon\Phi_{NL}) = (1 - \Phi_{NL})(1 - \varepsilon\Phi_{NL})$ as derived in the Supporting Information (Eq. S1). Therefore, the sDNA volume fraction may be written as

$$ {\Phi_V}^{sDNA} = {\Phi_V}^{sDNA}(\Phi_{CL} = 1)[(1 - \Phi_{NL})(1 - \varepsilon\Phi_{NL})] \qquad (2) $$

To calculate ${\Phi_V}^{sDNA}(\Phi_{CL} = 1)$ from eq 1, we use a_{bp} = (3.4 Å)(20 Å) = 68 Å^2 and a_{CL} = 70 Å^2, which for $\rho_{chg} = 1$ (stoichiometrically neutral complexes) and $Z_{CL} = 1$ (univalent DOTAP) leads to ${\Phi_V}^{sDNA}(\Phi_{CL} = 1) \approx 0.97$. Further simplification is possible because $(1 - \varepsilon\Phi_{NL})$ ranges between 1 and 0.98 for $0 \leq \Phi_{NL} \leq 0.7$ (using a_{NL} = 72 Å^2,[35] which gives $\varepsilon = r - 1 = 0.029$). Thus, the following simple relationship between the

dx.doi.org/10.1021/ja202082c |J. Am. Chem. Soc. 2011, 133, 7585–7595

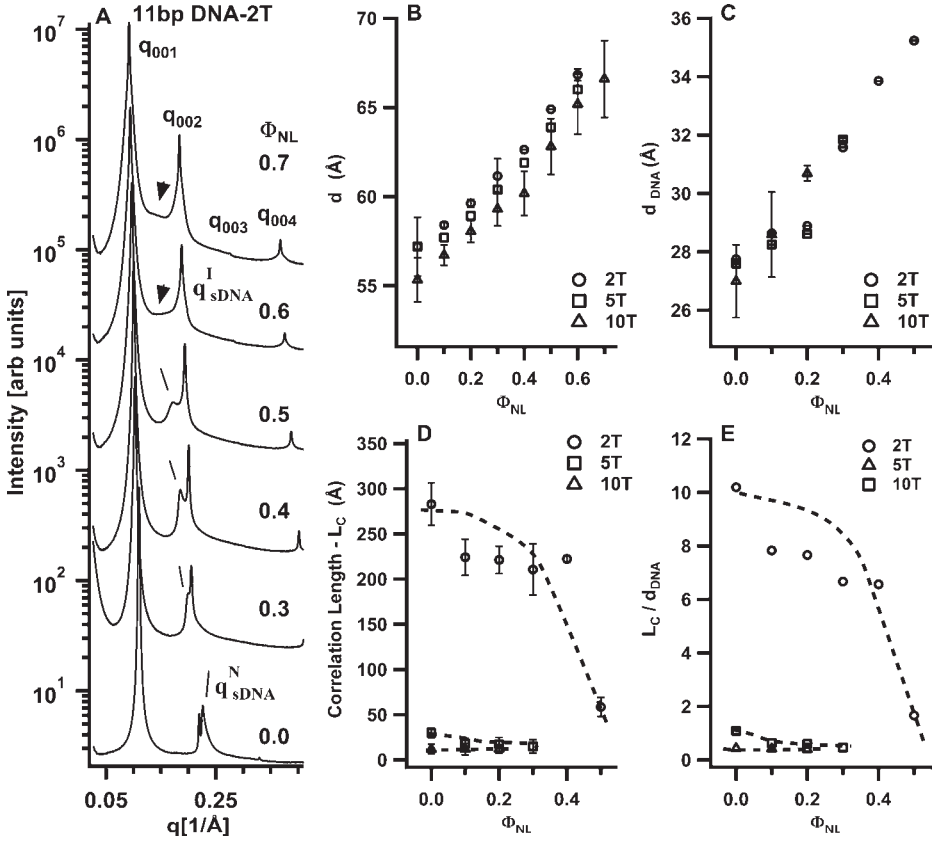

Figure 8. (A) Synchrotron SAXS profiles of CL−sDNA complexes containing 11 bp DNA with 2-T nonsticky overhangs (11 bp DNA-2T) as a function of neutral lipid mole fraction (Φ_{NL}). The (00L) diffraction peaks result from the multilamellar structure of the complexes. Lines point to relatively sharp sDNA−sDNA correlation peaks, indicative of the new type of columnar nematic phase (Figure 1C) as described in the text. Arrows point to broad sDNA peaks characteristic of the isotropic phase. (B−E) Plots of the interlayer spacing d (B), the average spacing between sDNA molecules d_{DNA} (C), the correlation length L_C (D), and L_C in units of d_{DNA} (E) as a function of Φ_{NL} for CL−sDNA complexes containing 11 bp DNA-2T (open circles) and, for comparison, 11 bp DNA-5T (open squares) and 11 bp DNA-10T (open triangles). The parameters result from line shape fits of the q_{002} and q_{sDNA} peaks in the SAXS profiles of the corresponding complexes with a double Lorentzian. The observed values of L_C (D) and L_C/d_{DNA} (E) for 11 bp DNA-2T show a highly correlated nematic phase with L_C/d_{DNA} ranging between 6 and 10, in contrast to the isotropic phase with $L_C/d_{DNA} < 1$ observed for 11 bp DNA-10T and 11 bp DNA-5T. This new phase undergoes a transition to the isotropic phase for $\Phi_{NL} > 0.5$ (where L_C/d_{DNA} decreases to ~1). The building blocks of this highly correlated nematic phase (labeled columnar nematic, N_C) are 1D stacks of 11 bp DNA-2T rods that result from the onset of strong sDNA end-to-end interactions. Applying Onsager's criterion to this phase gives an estimate of the stack length as on average four rods, as shown in Figure 1C.

sDNA volume fraction and Φ_{NL} results:

$$\Phi_V^{sDNA} \approx 0.97[(1-\Phi_{NL})(1-\varepsilon\Phi_{NL})] \approx 0.97(1-\Phi_{NL}) \quad (3)$$

Comparison with Onsager's Model. We can now use eq 3 to compare the predictions of Onsager's model to the data shown in Figure 5D. As described in the Introduction, Onsager's theory predicts that the I-to-N phase transition should occur for rod volume fractions $\Phi_V^{rod} \geq 4D/L$ for hard-core repulsive anisotropic rods.[11] For 48 bp DNA-10T, $L/D \approx 8.16$, which implies that the N phase should be observed for $\Phi_V^{sDNA} \geq 0.49$ or equivalently for $\Phi_{NL} \leq 0.495$. The data in Figure 5D show that L_C/d_{DNA} is between 2 and 4 for $\Phi_{NL} \leq 0.50$, indicating a N phase. The transition to the I phase occurs at Φ_{NL} between 0.5 and 0.6, where L_C/d_{DNA} drops below 1 (signifying little correlations between neighboring sDNA molecules). This is qualitatively consistent with the Onsager model because the addition of the 10-T overhangs effectively increases the length-to-width anisotropy over the L/D of the 48 bp core, which in turn would extend the range of Φ_{NL} over which the N phase is stable. For 11 bp DNA-10T, $L/D \approx 2$, and the N phase is not expected to be stable for any sDNA volume fraction. This is consistent with the observation of very weak correlations, $L_C/d_{DNA} < 1$ (Figure 5D, open triangles), over the small Φ_{NL} range where the broad sDNA−sDNA correlation peak is observable (Figure 3A). For 24 bp DNA-10T, L_C/d_{DNA} extends between one and two neighbors (Figure 5D, open squares) for $\Phi_{NL} < 0.3$. For $\Phi_{NL} > 0.3$, the absence of sDNA−sDNA correlation peaks is indicative of the I phase (Figure 3B). Such a small L_C/d_{DNA} is consistent with a very weak N phase and a N−I transition near $\Phi_{NL} \approx 0.3$ or $\Phi_V^{sDNA} \approx 0.68$ (from eq 3). Using this value and the Onsager model gives an effective $L/D \approx 5.9$, which is qualitatively consistent with the relatively long 10-T overhangs extending L/D by about 50% beyond that of the 24 bp core with $L/D \approx 4.08$.

We would like to stress that computer simulations have shown that the precise shape of the ends of anisotropic rods is a major factor in determining the critical rod volume fraction at which the N phase becomes stable.[12,13] Thus, a more quantitative comparison between our experimental results and theoretical predictions

dx.doi.org/10.1021/ja202082c |*J. Am. Chem. Soc.* 2011, 133, 7585–7595

would require simulations of sDNA rods with ends comprised of dangling unstructured overhangs. Nevertheless, the observation of an N phase ordering for 24 and 48 bp DNA with 10-T nonsticky ends, and the absence of N phase for 11 bp DNA-10T, all of which are at least qualitatively consistent with Onsager theory, are a strong indication that the relatively long 10-T nonsticky overhangs suppress the DNA end-to-end interactions observed in blunt DNA.[15,16] Interestingly, SAXS experiments show that a small degree of DNA end-to-end interactions begins to set in for 24 and 48 bp DNA duplexes as the nonsticky overhangs are reduced in length.

Effect of the Length of Nonsticky Overhangs on the Phase Behavior of Longer sDNAs. To highlight the effect of the three different lengths of nonsticky overhangs, Figures 6 and 7 plot the structural parameters of CL complexes of the studied 24 and 48 bp DNA duplexes, respectively, as a function of Φ_{NL}. As for Figure 5, these parameters (d, d_{DNA}, L_C, and L_C/d_{DNA}) result from fits of the SAXS profiles to Lorentzian X-ray structure factors. As expected, the values for d and d_{DNA} are nearly unaffected by the length of the nonsticky overhangs (Figures 6A,B and 7A,B). Most significantly, the values of Φ_{NL} for which the sDNA−sDNA correlation lengths L_C (Figures 6C and 7C) and L_C/d_{DNA} (Figures 6D and 7D) show a transition from the N to the I phase (with L_C/d_{DNA} decreasing rapidly from ∼3 or 4 to below 1) increase for duplexes with 5- and 2-T overhangs. Specifically, 24 bp DNA-2T duplexes are in the N phase for Φ_{NL} = 0.5 and 0.6, while 24 bp DNA-5T duplexes are in the I phase (Figure 6D); similarly, 48 bp DNA-2T duplexes are in the N phase at Φ_{NL} = 0.6, while the corresponding duplexes with 5- and 10-T overhangs are in the I phase (Figure 7D). Thus, the N−I phase transition occurs at smaller sDNA volume fractions as the length of the overhangs on the 24 and 48 bp sDNA molecules decreases from 10 to 5 and 2 T. Applying Onsager's condition for nematic ordering ($\Phi_V^{rod} \geq 4D/L$), this implies that the effective L/D increases slightly with decreasing overhang length. This in turn is consistent with the onset of a small amount of attractive end-to-end interactions for 24 and 48 bp DNA duplexes. These interactions would lead to the formation of transient dimers from some of the duplexes with the shorter 5- and 2-T overhangs, resulting in a larger effective (average) rod length. In contrast to these weak end-to-end interactions, where the LC phase behavior is dominated by the anisotropic shape of the sDNA rods, 11 bp DNA duplexes with 2-T overhangs exhibit very strong sDNA end-to-end stacking interactions, which lead to a new type of 2D nematic LC phase, as we describe below.

End-to-End Stacking Interactions Lead to Columnar Nematic (N_C) Liquid Crystal Phase Formation for 11 bp DNA Duplexes with Nonsticky 2-T Overhangs. *SAXS Studies: Observation of the Columnar Nematic (N_C) Liquid Crystal Phase.* Figure 8A shows SAXS profiles for DOTAP/DOPC−sDNA complexes incorporating 11 bp DNA-2T as a function of the neutral lipid mole fraction Φ_{NL}. The very sharp (00L) diffraction peaks again result from the multilamellar structure of the complexes. However, in striking contrast to the SAXS profiles of Figure 3A (showing data for 11 bp DNA-10T with long nonsticky ends), relatively sharp sDNA−sDNA correlation peaks are visible (lines point to the peaks in Figure 8A). The 11 bp DNA-10T molecules exhibited only the I phase, with very broad q_{sDNA} SAXS peaks. The sharper sDNA peaks for 11 bp DNA-2T duplexes indicate the onset of strong end-to-end stacking interactions because $L/D \approx 1.9$ for 11 bp DNA-2T is well below the Onsager criterion for N phase ordering. As before, the q_{002} and q_{sDNA} peaks were fit to a double Lorentzian X-ray structure factor in order to quantitatively obtain the structural parameters displayed in Figure 8B−E. Figure 9 shows an example of such a fit for Φ_{NL} = 0.5. Figure 9A plots part of the SAXS profiles and background (dashed line), and Figure 9B plots the fit of the background-subtracted SAXS profile to the double Lorentzian line shape (solid line). Again, the q^N_{sDNA} peaks fit quantitatively to Lorentzian line shapes. This indicates that the sDNA molecules are indeed in the nematic phase but with strongly enhanced short-range positional order because the q^N_{sDNA} profiles in Figure 8A are narrower than those in Figure 3B,C.

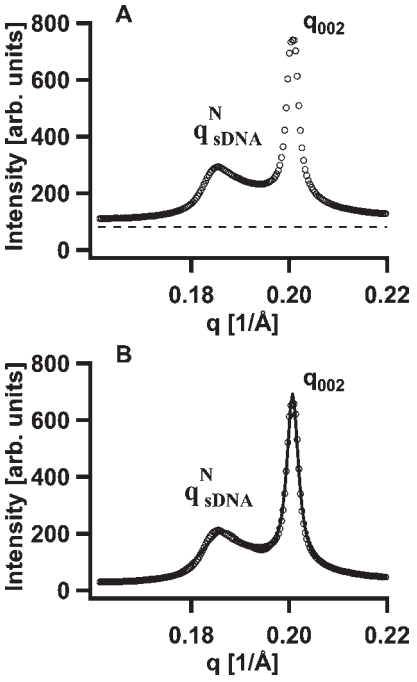

Figure 9. (A) Part of the SAXS profile of CL−sDNA complexes incorporating 11 bp DNA-2T at Φ_{NL} = 0.5 (cf. Figure 8A). The dashed line shows the background scattering, which was approximated as an exponential decay fit through the X-ray intensity far from the diffraction peaks. (B) A nonlinear least-squares fit of the background-subtracted SAXS profile from part A (open circles) with the sum of two Lorentzians (solid line). Each Lorentzian function was written as $S(q) = A/[(q - q_o)^2 + \kappa^2]$, where q_o and κ correspond to the peak position and the hwhm, respectively. For the (002) SAXS peak, $A_{002} = 5.16 \times 10^{-3}$, q_{002} = 0.2007 Å^{-1}, and $\kappa_{002} = 1.44 \times 10^{-3}$ Å^{-1}, and for the q^N_{sDNA} SAXS peak (due to sDNA−sDNA correlations), $A_{sDNA} = 2.15 \times 10^{-2}$, q_{sDNA} = 0.1856 Å^{-1}, and $\kappa_{sDNA} = 4.50 \times 10^{-3}$ Å^{-1}.

The interlayer spacing d, plotted together with the data for 11 bp DNA-5T and 11 bp DNA-10T in Figure 8B, shows the expected increase with increasing Φ_{NL} (see above, discussion of Figure 5A). Figure 8C shows that d_{DNA} for 11 bp DNA-2T increases as expected with increasing Φ_{NL} (i.e., decreasing cationic membrane charge density; see discussion of Figure 5B). Figure 8D and E plots the correlation length L_C and L_C/d_{DNA}, respectively, for 11 bp DNA-2T and, for comparison, for 11 bp DNA-5T and 11 bp DNA-10T. For 11 bp duplexes with 10- and 5-T overhangs, $L_C/d_{DNA} < 1$, independent of Φ_{NL}, indicative of the isotropic phase with weak positional correlations. In contrast, L_C/d_{DNA} for 11 bp DNA-2T dramatically increases for $\Phi_{NL} \leq 0.4$, with correlations extending between ∼6 and ∼8 neighbors.

The N_C−I Phase Transition Reveals Finite-Size sDNA Stacks. The N−I phase transition occurs near Φ_{NL} = 0.5 (with $L_C/d_{DNA} \approx 1$), equivalent to a sDNA volume fraction of ∼0.49. This

dx.doi.org/10.1021/ja202082c |J. Am. Chem. Soc. 2011, 133, 7585–7595

indicates the presence of sDNA end-to-end interactions for 11 bp duplexes with the smallest 2-T overhangs, which lead to the stacking of the 11 bp DNA-2T rods with an average $L_{STACK}/\Phi^{*sDNA}_{V} \approx 4/0.49 = 8.2$. The building blocks of this novel 2D columnar nematic phase (N_C, shown schematically in Figure 1C) consist of 1D stacks of sDNA, which are comprised of an average of four 11 bp DNA-2T molecules (where the 11 bp core has $L/D \approx 1.9$). We point out that the stacking is expected to be dynamic; i.e., 11 bp DNA-2T rods may readily associate with and dissociate from 1D stacks.

The observation that 11 bp DNA-2T molecules exhibit much larger end-to-end stacking interactions than 24 and 48 bp DNA-2T rods is unexpected. This difference in behavior may be related to the fact that 11 bp DNA is well approximated by a rigid rod, whereas 48 bp DNA (having a length (~163 Å) of order one-third of the persistence length of DNA (~ 500 Å)) is more flexible (the same is true for 24 bp DNA, although to a lesser extent). Thermal fluctuations would tend to more easily break the end-to-end interactions of slightly bent rods. For example, rotations about the cylinder axis of rigid rods would leave the end-to-end interactions unchanged, while similar rotations at different points along the contour of a bent rod would tend to break the stacking.

CONCLUSIONS

The environment between lipid layers in CL−DNA complexes provides a unique way to study 2D confinement effects on anisotropic nanorods in the context of self-assembled structures. Our results show that short DNA rods confined within the membranes of CL−sDNA complexes exhibit rich LC phase behavior. We focused on 11, 24, and 48 bp DNA duplexes with nonpairing 2-, 5-, and 10-T overhangs. The addition of the single-stranded overhangs to the double-stranded DNA core introduced a steric repulsion, which reduced the recently discovered DNA end-to-end stacking effect[15] to a degree varying with the length of the nonpairing overhangs. The core duplexes' length-to-width ratios, $L/D \approx 1.87$, 4.08, and 8.16, provided examples of rods with shape anisotropies below (11 bp), near (24 bp), and above (48 bp) the Onsager condition for nematic LC ordering. In combination with the varying overhang length, this allowed us to discern nematic LC ordering of sDNA due to Onsager anisotropic shape effects (24 and 48 bp DNA-10T) from end-to-end stacking effects (11 bp DNA-2T). In the former (Onsager) regime, shortening the overhang lengths for 24 and 48 bp duplexes to 5- and 2-T moderately enhanced the range of stability for the nematic phase, indicating some end-to-end interactions. In the latter (stacking) regime, the onset of strong end-to-end interactions for 11 bp DNA-2T resulted in the formation of a new type of columnar nematic phase, where the nematically ordered building blocks consist of 1D stacks of sDNA molecules with an estimated average stack length of four sDNA molecules.

It is interesting to speculate on the possibility of a corresponding 3D columnar nematic phase with finite-length columns. Because thermal fluctuations are substantially reduced in going from 2D to 3D,[1,2] sDNA duplexes with 2-T overhangs may exhibit complete stacking of the duplexes in 3D (i.e., with column lengths of the order of the size of the sample container). Generating a 3D equivalent of the 2D nematic columnar phase with finite-length columns observed on cationic membranes may require longer nonpairing overhangs (between 2- and 5-T) to further weaken the end-to-end stacking interactions.

Our results may be applied in the design of optimally packed LC phases of anisotropic rods (including short RNA or peptides) in CL-based complexes, which is of special interest because CLs have broad applications as carriers of therapeutic macromolecules.[4,19,20,37] The results reported here indicate that creating columns of stacked siRNA molecules through end-to-end interactions should improve the packing efficiency within CL−siRNA complexes and in turn allow more siRNA to be delivered per lipid.[3,4] However, we should caution that the stability of stacked RNA duplexes in a cellular environment is not known. Importantly, if duplexes remain stacked within a cell, they may be recognized by host defense mechanisms and trigger innate immune responses.[38]

While the structures of CL−DNA complexes with long DNA have been studied in great detail experimentally[5−10,39] as well as theoretically[40−45] and in recent simulations,[46] the rich phase behavior described in this paper should motivate future simulations of the structure and phase behavior of short DNA and other rod-like molecules such as siRNAs or peptides, confined within an aqueous 2D environment. In particular, we expect our findings and future computer simulations to stimulate designs of DNA-directed assembly on robust 2D platforms through end-to-end interactions.

ASSOCIATED CONTENT

Supporting Information. Sequences of the sense and antisense strands of the studied sDNA and derivations as mentioned in the text. This material is available free of charge via the Internet at http://pubs.acs.org.

AUTHOR INFORMATION

Corresponding Author
Safinya@mrl.ucsb.edu

Present Addresses
[#]Mucosal Immunology, M.F. Kagnoff Laboratory, Department of Medicine, University of California, San Diego.

ACKNOWLEDGMENT

N.F.B., K.K.E., Y.L., and C.R.S. were supported by NIH GM-59288, DOE-BES grant no. DOE-DE-FG02-06ER46314 (DNA liquid crystalline assembly), and NSF DMR-0803103. C.L. was funded by the Swedish Research Council (VR) and in part by DOE-BES. C.S.M. and C.E.S. were supported by NIH AI-12520 and AI-20611. The X-ray diffraction work was carried out at the Stanford Synchrotron Radiation Lightsource (SSRL), beamline 4-2, supported by the DOE. C.R.S. acknowledges a World Class University Visiting Professor of Physics appointment supported by the National Research Foundation of Korea, funded by the Ministry of Education, Science and Technology grant no. R33-2008-000-10163-0.

REFERENCES

(1) De Gennes, P. G.; Prost, J. *The Physics of Liquid Crystals*, 2nd ed.; Oxford University Press: Oxford, 1993.

(2) Chaikin, P. M.; Lubensky, T. C. *Principles of Condensed Matter Physics*; Cambridge University Press: Cambridge, 1995.

(3) Bouxsein, N. F.; McAllister, C. S.; Ewert, K. K.; Samuel, C. E.; Safinya, C. R. *Biochemistry* **2007**, *46*, 4785–4792.

(4) Ewert, K. K.; Zidovska, A.; Ahmad, A.; Bouxsein, N. F.; Evans, H. M.; McAllister, C. S.; Samuel, C. E.; Safinya, C. R. *Top. Curr. Chem.* **2010**, *296*, 191–226.
(5) Rädler, J. O.; Koltover, I.; Salditt, T.; Safinya, C. R. *Science* **1997**, *275*, 810–814.
(6) Lin, A. J.; Slack, N. L.; Ahmad, A.; George, C. X.; Samuel, C. E.; Safinya, C. R. *Biophys. J.* **2003**, *84*, 3307–3316.
(7) Salditt, T.; Koltover, I.; Rädler, J.; Safinya, C. R. *Phys. Rev. Lett.* **1997**, *79*, 2582–2585.
(8) Salditt, T.; Koltover, I.; Rädler, J. O.; Safinya, C. R. *Phys. Rev. E* **1998**, *58*, 889–904.
(9) Koltover, I.; Salditt, T.; Safinya, C. R. *Biophys. J.* **1999**, *77*, 915–924.
(10) Zidovska, A.; Evans, H. M.; Ahmad, A.; Ewert, K. K.; Safinya, C. R. *J. Phys. Chem.* **2009**, *113*, 5208–5216.
(11) Onsager, L. *Ann. N.Y. Acad. Sci.* **1949**, *51*, 627–659.
(12) Bolhuis, P.; Frenkel, D. *J. Chem. Phys.* **1997**, *106*, 666–685.
(13) Cuesta, J. A.; Frenkel, D. *Phys. Rev. A* **1990**, *42*, 2126–2136.
(14) Bates, M.; Frenkel, D. *J. Chem. Phys.* **2000**, *112*, 10034–10041.
(15) Nakata, M.; Zanchetta, G.; Chapman, B. D.; Jones, C. D.; Cross, J. O.; Pindak, R.; Bellini, T.; Clark, N. A. *Science* **2007**, *318*, 1276–1279.
(16) Zanchetta, G.; Bellini, T.; Nakata, M.; Clark, N. A. *J. Am. Chem. Soc.* **2008**, *130*, 12864–12865.
(17) Strzelecka, T. E.; Davidson, M. W.; Rill, R. L. *Nature* **1988**, *331*, 457–460.
(18) Livolant, F.; Levelut, A. M.; Doucet, J.; Benoit, J. P. *Nature* **1989**, *339*, 724–726.
(19) *Delivery Technologies for Biopharmaceuticals: Peptides, Proteins, Nucleic Acids and Vaccines*; Jorgensen, L., Nielsen, H. M., Eds.; John Wiley & Sons: New York, 2009.
(20) Kim, D.-H.; Behlke, M. A.; Rose, S. D.; Chang, M.-S.; Choi, S.; Rossi, J. J. *Nat. Biotechnol.* **2005**, *23*, 222–226.
(21) Mirkin, C. A.; Letsinger, R. L.; Mucic, R. C.; Stohrhoff, J. J. *Nature* **1996**, *382*, 607–609.
(22) Elghanian, R.; Stohrhoff, J. J.; Mucic, R. C.; Letsinger, R. L.; Mirkin, C. A. *Science* **1997**, *277*, 1078–1081.
(23) Nykypanchuk, D.; Maye, M. M.; van der Lelie, D.; Gang, O. *Nature* **2008**, *451*, 549–552.
(24) Maye, M. M.; Nykypanchuk, D.; van der Lelie, D.; Gang, O. *J. Am. Chem. Soc.* **2006**, *128*, 14020–14021.
(25) Seeman, N. C. *Nature* **2003**, *421*, 427–431.
(26) Elbashir, S. M.; Harborth, J.; Lendeckel, W.; Yalcin, A.; Weber, K.; Tuschl, T. *Nature* **2001**, *411*, 494–498.
(27) Caille, C. R. *C. R. Seances Acad. Sci., Ser. B* **1972**, *274*, 891–893.
(28) Als-Nielsen, J.; Litster, J. D.; Birgeneau, R. J.; Kaplan, M.; Safinya, C. R.; Lindegaardandersen, A.; Mathiesen, S. *Phys. Rev. B* **1980**, *22*, 312–320.
(29) Safinya, C. R.; Roux, D.; Smith, G. S.; Sinha, S. K.; Dimon, P.; Clark, N. A.; Bellocq, A. M. *Phys. Rev. Lett.* **1986**, *57*, 2718–2721.
(30) Landau, L. D. In *Collected Papers of L. D. Landau*; Ter Haar, D., Ed.; Gordon and Breach: New York, 1965.
(31) Peierls, R. E. *Helv. Phys. Acta Suppl.* **1934**, *7*, 81–83.
(32) Davidov, D.; Safinya, C. R.; Kaplan, M.; Dana, S. S.; Schaetzing, R.; Birgeneau, R. J.; Litster, J. D. *Phys. Rev. B* **1979**, *19*, 1657–1663.
(33) Garland, C. W.; Meichle, M.; Ocko, B. M.; Kortan, A. R.; Safinya, C. R.; Yu, L. J.; Litster, J. D.; Birgeneau, R. J. *Phys. Rev. A* **1983**, *27*, 3234–3240.
(34) Safinya, C. R.; Birgeneau, R. J.; Litster, J. D.; Neubert, M. E. *Phys. Rev. Lett.* **1981**, *47*, 668–671.
(35) Ahmad, A.; Evans, H. M.; Ewert, K.; George, C. X.; Samuel, C. E.; Safinya, C. R. *J. Gene Med.* **2005**, *7*, 739–748.
(36) Bruinsma, R. *Eur. Phys. J. B.* **1998**, *4*, 75–88.
(37) Leal, C.; Bouxsein, N. F.; Ewert, K. K.; Safinya, C. R. *J. Am. Chem. Soc.* **2010**, *132*, 16841–16847.
(38) Samuel, C. E. *Clin. Microbiol. Rev.* **2001**, *14*, 778–809.
(39) Artzner, F.; Zantl, R.; Rapp, G.; Rädler, J. *Phys. Rev. Lett.* **1998**, *81*, 5015–5018.
(40) Harries, D.; May, S.; Gelbart, W. M.; Ben-Shaul, A. *Biophys. J.* **1998**, *75*, 159–173.
(41) Golubović, L.; Golubović, M. *Phys. Rev. Lett.* **1998**, *80*, 4341–4344.
(42) O'Hern, C.; Lubensky, T. *Phys. Rev. Lett.* **1998**, *80*, 4345–4348.
(43) Golubović, L.; Lubensky, T.; O'Hern, C. *Phys. Rev. E* **2000**, *62*, 1069–1094.
(44) May, S.; Harries, D.; Ben-Shaul, A. *Biophys. J.* **2000**, *78*, 1681–1697.
(45) Harries, D.; May, S.; Ben-Shaul, A. *J. Phys. Chem. B* **2003**, *107*, 3624–3630.
(46) Farago, O.; Grønbech-Jensen, N. *J. Am. Chem. Soc.* **2009**, *131*, 2875–2881.